Journal of Agricultural Science and Technology (JAST), 28(2)
In Press, Pre-Proof Version

Non-Invasive Detection of Early Germination in Beans Using Laser Speckle Temporal Analysis and Deep Learning

Eli Veiga Junior[1], Sidnei Alves de Araújo[1]*, and Alessandro Melo Deana[1, 2]

ABSTRACT

The visual quality control of bean grains is currently conducted manually and relies heavily on identifying surface-level defects to classify the product type. Among these defects, germinated grains pose a unique challenge: in their early stages, germination is not externally visible, requiring invasive methods such as physically breaking the seed for detection. This study proposes a non-invasive and automated approach that combines laser speckle imaging with deep learning to identify early-stage germinated defects in beans. Speckle images were captured under coherent laser illumination (λ = 633 nm) for samples subjected to germination periods of 0, 6, 12, and 24 hours. Two contrast analysis techniques were evaluated: Laser Speckle Spatial Contrast Analysis (LASCA) and the more advanced Laser Speckle Temporal Contrast Analysis (LASTCA), the latter using temporal intensity fluctuations across 120 video frames. From the resulting contrast maps, regions of interest (50×50 pixels) were extracted and used to train a Convolutional Neural Network (CNN) for binary classification. The proposed system achieved high performance, with an accuracy of 92.33% and sensitivity of 98.21%, successfully detecting germinated defects invisible to conventional inspection. By integrating temporal biospeckle analysis with deep learning, this method offers a scalable solution for intelligent, non-destructive grain inspection—addressing a critical gap in current computer vision systems and contributing to the advancement of Agribusiness 4.0.

Keywords: Laser Speckle image, Computer Vision, Convolutional Neural Network, Bean, Germinated.

1. INTRODUCTION

Given the significant market demand for grains, including beans, agroindustries have directed their investments toward advanced technological innovations, driven by the imperative need to maintain a competitive position in the current socioeconomic landscape. These initiatives

[1] Informatics and Knowledge Management Post-Graduation Program, Nove de Julho University (UNINOVE), Vergueiro Street 235/249, São Paulo 01504-001, Brazil.
[2] Biophotonics Applied to Health Sciences Graduate Program, Nove de Julho University (UNINOVE), Vergueiro Street 235/249, São Paulo 01504-001, Brazil.
Corresponding author; e-mail: saraujo@uni9.pro.br

primarily aim to satisfy the evolving preferences of consumers while simultaneously committing to the production of safe and high-quality food products. The implementation of these technological innovations has enabled companies to minimize waste, maximize profits, reduce dependence on manual inspections, optimize productivity on a broad scale, capture new markets, and enhance organizational performance [1].

Quality control and inspection tasks for agricultural products aim to ensure that they are free from abnormal odors, moisture, foreign bodies, impurities, pest infestations, and mechanical damage, guaranteeing their safe delivery to consumers [2,3].

Nowadays, the inspection of bean grains is still conducted manually using a minimum 1 kg sample extracted from a batch of the product. Initially, foreign objects such as insects, stones, and impurities are separated using a sieve with circular openings measuring five millimeters in diameter. Subsequently, the beans are categorized into Group, Class, and Type. The Group pertains to the botanical species, while the Class is determined based on the color of the bean hulls (Black, White, Colored, or Mixed), regardless of the group. Finally, the Type is defined according to the maximum tolerance limits for defects (split, scorched, moldy, deformed, impurities, foreign matter, and germinated beans) found in the inspected sample [3].

The “germinated” defect, in its early stage, can only be detected through invasive methods that involve physically breaking the grain to enable visualization, rendering them unsuitable for consumption after such analyses. Therefore, despite computer vision playing a crucial role in the non-invasive assessment of the quality of agricultural products through the identification of visual patterns, it, like human vision, is incapable of detecting the germinated defect. As an example, consider the work of Belan *et al.* [4] in which they proposed a computer vision system (CVS) for inspecting the quality of bean grains, capable of detecting some defects (deformed, broken, scorched, and moldy), but notably excluding germinated beans. In this context, a non-invasive alternative lies in the laser speckle imaging analysis methods, which have already been applied in the analysis of seeds and agricultural grains. For instance, such methods have been used to identify genetic characteristics, patterns related to storage, and seed viability for planting purposes.

The phenomenon of speckle is elucidated as an optical interference occurrence that materializes when coherent light, such as laser emissions, undergoes dispersion subsequent to its interaction with a physical medium. At first glance, a speckle pattern may seem like a random cluster of bright

and dark spots, nevertheless it carries information on the surface and sub-surface characteristics of the sample [5-12].

Silva *et al.* [13], Peixoto *et al*. [14], Xia *et al*. [15], and Singh *et al.* [16] have conducted studies with the aim of demonstrating that speckle can be advantageously employed as an efficient, non-destructive, and cost-effective tool for analyzing seeds and grains, ultimately enhancing germination properties and productivity. Silva *et al.* [13] proposed to investigate the treatment of pathogens using bioprotectants in maize seeds, both immediately after and during storage. Peixoto *et al.* [14] applied biospeckle to discern microbial activity in maize seeds through the generation of activity maps via Laser Speckle Contrast Analysis (LASCA). Xia *et al*. [15] conducted a literature review on emerging technologies for seed viability analysis in cultivation, sales, and planting contexts. Singh et al. [16] explored the application of biospeckle in characterizing pre-sowing treatments as a cost-effective approach to improve seed germination properties and productivity.

Kurokawa *et al.* [17] and Contado *et al*. [18] have collectively affirmed that speckle techniques, when coupled with numerical analysis, can effectively be employed to monitor biological activity throughout the germination process. In this context, Singh *et al.* [19] and Thakur *et al*. [20] conducted biospeckle analyses to track the germination process, aiming to assess the viability and vigor of both bean and soybean seeds. Their findings collectively underscore the significant potential of this non-invasive technique.

In earlier yet pertinent studies concerning the present research, such as those conducted by Braga *et al.* [21] and Rabelo *et al*. [22], it was ascertained through biospeckle analysis that fungal activities exhibited notable distinctions between inoculated and non-inoculated bean seeds.

Indeed, it is worth noting that the majority of studies in laser speckle image analysis have relied on the traditional classical Statistical Theory, a framework developed several decades ago, as pointed by Goodman and his contemporaries [23].

Laser speckle image analysis holds the potential to extract valuable information from samples and correlate patterns with specific conditions. However, it's important to note that the analysis and classification of these patterns are currently conducted manually by a trained technician. This manual approach, while effective, can be labor-intensive and subject to interobserver variability. Hence, there is a growing interest in automating and enhancing this process through advanced

computational techniques, such as machine learning and deep learning, to improve efficiency, accuracy, and consistency in pattern recognition and classification tasks.

In this research, we break new ground by introducing state-of-the-art artificial intelligence techniques to the analysis of laser speckle images. Specifically, we employ these modern AI techniques to automate the classification of different types of bean grains, marking a significant advancement in the field of visual quality control of grains, promoting digital transformation and agribusiness 4.0.

2. MATERIAL AND METHODS

2.1 Image Acquisition

Figure 1 shows the experimental setup used for this work for images and videos acquisition.

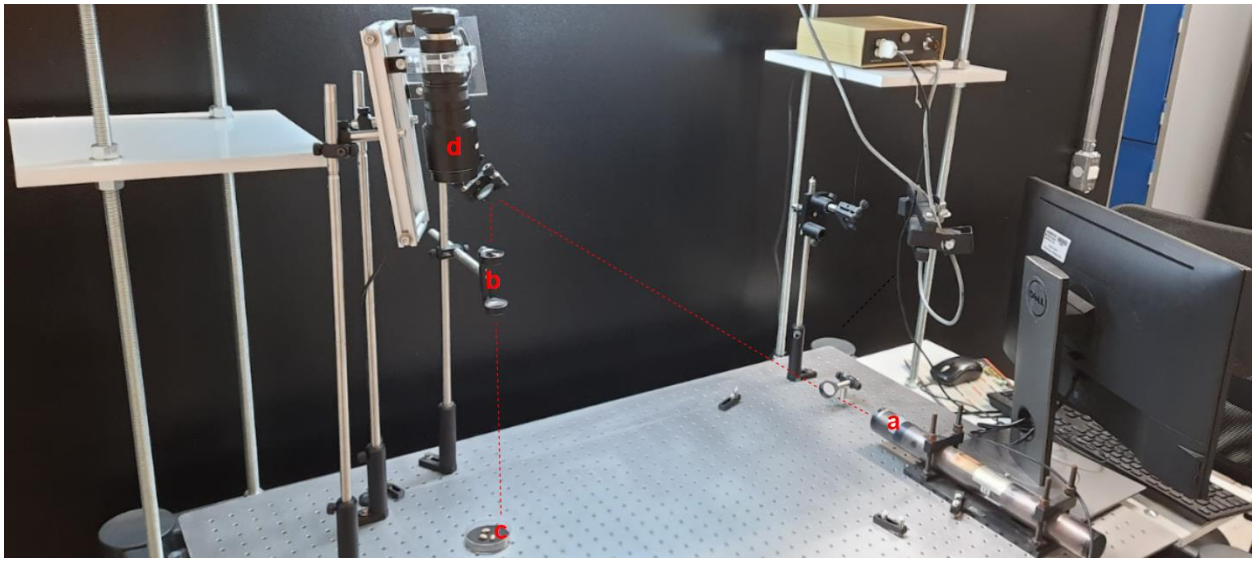

Figure 1. Experimental setup used in this work. (a) HeNe laser source at λ = 633 nm; (b) Beam expander; (c) Sample holder, (d) Image acquisition camera.

The laser bean was expanded to encompass uniform illumination throughout the entire sample while providing ample luminosity to activate the sensor of the photographic system, as outlined in [9].

The experimental setup was designed to enable non-invasive detection of early germination defects in bean grains using laser speckle imaging. A Helium-Neon (HeNe) laser emitting at 633 nm was chosen as the illumination source due to its high spatial and temporal coherence, stable output, and suitability for biological materials, making it ideal for generating high-contrast speckle patterns. To ensure uniform illumination across the entire surface of each bean sample, a beam

expander was employed, preventing localized intensity variations that could compromise speckle pattern formation and contrast quality.

As illustrated in Figure 1, image acquisition was carried out using a ThorLabs DCC1645C camera equipped with a sensor offering a resolution of 1280 × 1024 pixels, covering a physical area of 4.61 mm × 3.69 mm, with a pixel size of 3.6 µm². This high-resolution sensor enabled precise capture of spatial speckle features essential for detailed analysis. Since the laser source operated at a peak wavelength of $\lambda = 633$ nm, only the red channel of the camera sensor was used in processing to maximize the signal-to-noise ratio and ensure spectral compatibility. Importantly, no binning was applied during image acquisition, preserving the full spatial resolution of the sensor and enhancing the reliability of both spatial and temporal contrast computations.

For LASCA (Laser Speckle Spatial Contrast Analysis), a single static image was captured with an exposure time of 100 ms. For LASTCA (Laser Speckle Temporal Contrast Analysis), dynamic image sequences were recorded over 2 minutes at 25 frames per second, resulting in 3000 frames per sample, from which 120 frames were extracted for temporal analysis. Bean samples were prepared by exposing them to moisture using wet cotton pads for 6, 12, and 24 hours to induce progressive stages of germination, while the 0h group (control) remained dry to represent non-germinated grains.

This sample preparation protocol was designed to simulate real-world post-harvest scenarios while capturing subtle biological activity indicative of early germination. The resulting speckle contrast maps—whether spatial (LASCA) or temporal (LASTCA)—were used to extract 50×50-pixel regions of interest (ROIs), which were then fed into a convolutional neural network (CNN) for automated classification of germinated versus non-germinated beans. Every step in this process—from equipment selection to data acquisition—was carefully tailored to maximize speckle quality, reduce external noise, and support accurate, scalable, and real-time implementation of visual quality control in the agroindustry.

Figure 2 illustrates representative images of bean samples under two illumination conditions: (a) white light and (b) laser illumination, for each of the germination intervals investigated in this study. The time labels associated with the samples—0h, 6h, 12h, and 24h—correspond to the duration for which the beans were subjected to the germination process prior to image acquisition. Specifically, the 0h sample represents the control group, consisting of non-germinated beans that were not exposed to moisture, thereby serving as the reference condition. In contrast, the 6h, 12h,

and 24h samples correspond to beans undergoing progressive stages of germination, induced by controlled hydration over the specified time intervals. These images form the basis for subsequent speckle pattern analyses, enabling the assessment of dynamic biological activity associated with the germination process.

For each sample, a static image was acquired with an exposure duration of 100 milliseconds, followed by a video recording at 25 frames per second, with a total duration of 2 minutes. To optimize computational resources and focus solely on pertinent regions, we judiciously identified and processed exclusively the Regions of Interest (ROIs).

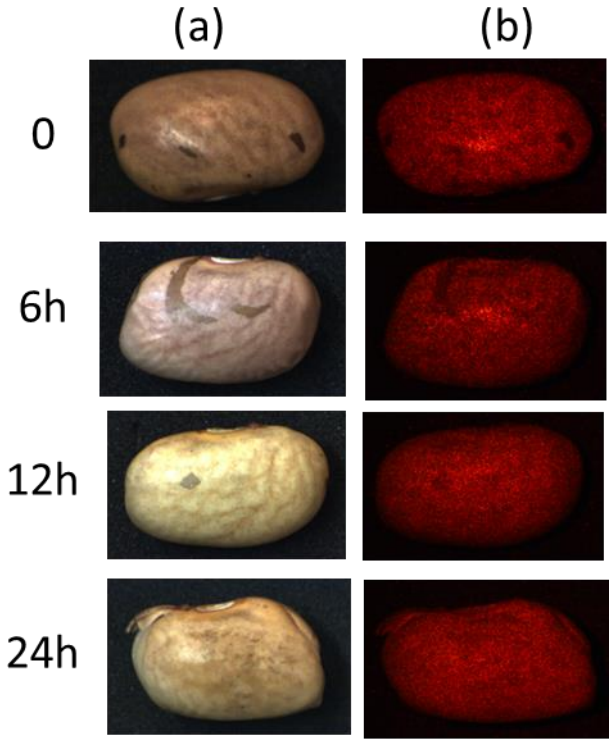

Figure 2. Samples under white illumination (a) and its laser speckle image counterpart (b) for germination intervals considered.

2.2 Laser speckle image analysis

The speckle phenomenon results from the interference of coherent light, such as a laser, scattered by a rough or dynamic surface. When the illuminated sample contains biological or biochemical activity—such as intracellular motion, water uptake, or metabolic activity—this leads to subtle, often imperceptible, temporal variations in the speckle pattern. The LASTCA method capitalizes on these dynamic changes by tracking the intensity fluctuations of individual pixels over time,

providing a temporal contrast map that reflects localized activity levels.

This approach builds upon findings in previous studies by Deana *et al.,* who demonstrated the capacity of laser speckle imaging to reveal subsurface or microstructural alterations in biological tissues and explain in detail the speckle phenomena [24 – 26]

Laser speckle contrast analysis

The Laser Speckle Spatial Contrast Analysis (LASCA) technique is a foundational method in speckle image processing, designed to quantify localized spatial variations in speckle patterns that arise from biological activity or structural heterogeneity on or beneath the surface of a sample. Unlike LASTCA, which explores intensity fluctuations over time, LASCA is based purely on the spatial distribution of intensity in a single speckle image, making it a suitable option for real-time or low-latency imaging scenario The laser speckle contrast analysis (LASCA) allows for the determination of various degrees of biological activity without the need for expensive equipment or extensive computational resources [23, 27].

The fundamental concept underpinning the LASCA method entails the partitioning each image into non overlapping square cells (or windows) of size 4×4 pixels (W=4). For each cell we calculate the mean and standard deviation, followed by the computation of contrast values (standard deviation divided by the mean). Each contrast was assigned to the central pixel of its corresponding cell generating a contrast map.

The LASCA method is implemented as follows:

1. **Image Acquisition**: A single static speckle image is acquired under laser illumination (λ = 633 nm). No temporal sequence is required.
2. **Image Partitioning**: The speckle image, with dimensions M×NM \times NM×N pixels, is divided into non-overlapping square windows of size W×WW \times WW×W pixels. In this study, a window size of **4×4 pixels** was adopted, following the recommendations from prior biomedical applications by Deana *et al*.[24]
3. **Statistical Contrast Calculation**: For each window, the spatial **mean intensity** μ and **standard deviation** σ are computed. The speckle **contrast** C is then defined as:

$$C(x,y) = \frac{\sigma(x,y)}{\mu(x,y)}$$

4. This dimensionless ratio quantifies the relative variation of intensity within the window, reflecting the degree of activity or heterogeneity in that region.
5. **Contrast Map Generation**: The computed contrast value is assigned to the **central pixel** of the corresponding window. Repeating this operation across all windows produces a **spatial contrast map**, where brighter areas correspond to higher contrast (i.e., greater local activity or scattering variability), and darker areas indicate lower contrast (more uniform or static regions).
6. **Map Interpretation and Classification**: The resulting LASCA map is used to extract 50×50-pixel regions of interest (ROIs), which are then classified by the CNN. These maps serve as the input for training and evaluating the deep learning model's ability to detect early-stage germination.

Laser Speckle Temporal Contrast Analysis (LASTCA)

The Laser Speckle Temporal Contrast Analysis (LASTCA) method shares similarities with LASCA, with a key distinction being its dynamic nature. In LASTCA, the contrast map is derived from a sequence of images acquired at different time intervals from each other. These time-separated images enable the assessment of how contrast values change over time, allowing for the observation of dynamic processes and temporal variations within the sample. This temporal aspect enhances the capability of LASTCA to capture and analyze dynamic phenomena, making it particularly valuable in applications where the temporal evolution of contrast is of interest, such as monitoring blood flow, particle dynamics, or other time-dependent processes [23].

In this particular case, rather than analyzing a square cell with neighboring pixels, the focus of analysis is on the statistical properties of an individual pixel at a specific position across different timeframes. In our study, a total of 16 images were acquired and overlapped for this purpose. This approach allows for the assessment of how the statistical characteristics of a single pixel at a fixed location evolve over time, providing valuable insights into the temporal dynamics and changes occurring within the sample. Figure 3 showcase de difference between LASCA and LASTCA.

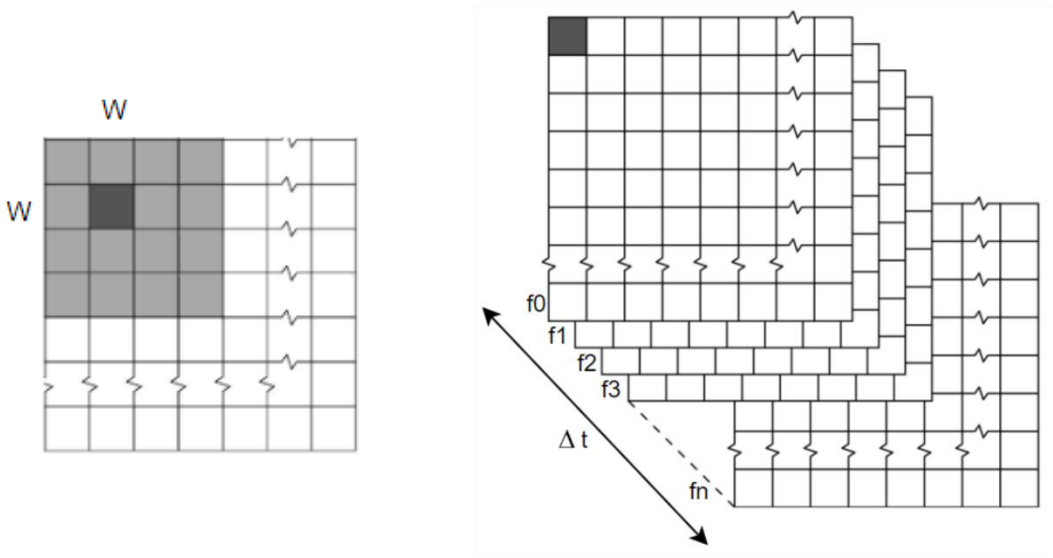

(a) (b)

Figure 3. Way of analyzing statistical properties in LASCA (a) and LASTCA (b).

The implementation of LASTCA in this work follows these core steps:

1. **Image Sequence Acquisition**: A sequence of 120 frames is acquired using a monochromatic (633 nm) laser source and a high-resolution CMOS sensor. Only the red color channel is analyzed to match the laser wavelength.
2. **Temporal Contrast Computation**: For each pixel at a fixed spatial coordinate (x, y), the temporal contrast $\mathbf{C_t}$ is computed over the intensity values $\mathbf{I_t}$ across all frames using:

$$C_t(x,y) = \frac{\sigma_t(x,y)}{\mu_t(x,y)}$$

   where σ_t and μ_t denote the temporal standard deviation and mean intensity of the pixel over time, respectively.
3. Contrast Map Generation: The resulting temporal contrast values are then assembled into a full-frame LASTCA map, where each pixel encodes the localized dynamic behavior over time.
4. Region Extraction and Classification: Sub-images (50×50 pixels) are extracted from the LASTCA maps and used to train a CNN, enabling automatic classification of germinated versus non-germinated grains

2.3 Proposed Method

The method proposed in this research receives as its input a collection of speckle images stored in an AVI file, representing frames (F) within a video, as visually depicted in Figure 4. The initial processing stage involves the isolation of the red band (R-band) from each individual frame (image of M×N pixels). Following this, the application of the LASTCA technique, which demonstrated notably superior performance in contrast to LASCA within comparative assessments, is executed on the ensemble of images representing the R-band across the frames. This process culminates in the derivation of detailed LASTCA maps calculated from batches of 120 frames (B=120), offering a refined depiction of the data's characteristics, and which feed the CNN to identify the defects in the grains.

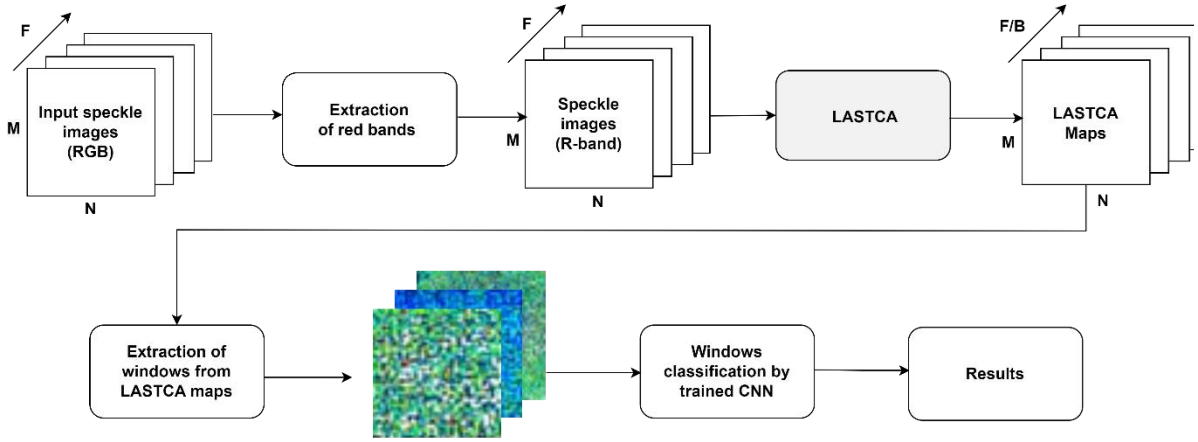

Figure 4. Flow of the proposed method.

Deep Learning

The CNN implemented in this study follows a sequential architecture and receives as input grayscale contrast maps of 50×50 pixels, as illustrated in Figure 5. The architecture begins with a rescaling layer to normalize pixel values to the [0,1] range, followed by two convolutional layers. The first convolutional layer uses 32 filters with a 3×3 kernel, 'same' padding, and ReLU activation, followed by a Batch Normalization and a MaxPooling2D layer to reduce spatial dimensions. The second convolutional layer includes 64 filters, also with a 3×3 kernel and ReLU activation, again followed by batch normalization and max pooling. The resulting feature maps are then flattened and passed through a dense layer with 128 neurons and ReLU activation, followed by a dropout layer with a rate of 0.2 to reduce overfitting. The final output layer consists of two neurons with sigmoid activation, for classification task. The model was compiled using the Adam

optimizer with a learning rate of 0.0001, and trained using cross entropy loss function with accuracy as the primary evaluation metric.

All training hyperparameters, including learning rate and other configuration choices, were defined based on preliminary experiments aimed at ensuring stable convergence, robustness, and generalization performance. In the data augmentation scenario, the number of training epochs was increased from 20 to 100 to ensure that the network had sufficient exposure to the significantly larger and more diverse dataset, as augmentation increases both the variability and volume of training data, which typically requires more iterations for the model to effectively learn and generalize the augmented patterns.

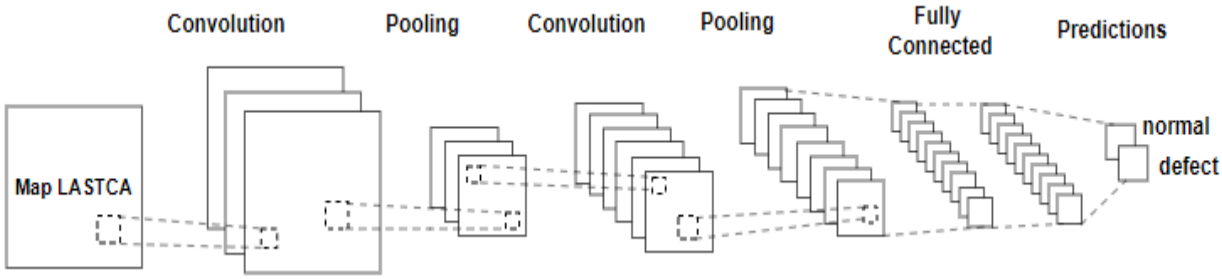

Figure 5. Architecture of the employed CNN.

After conducting the CNN training using the sets of sub-images with 50×50 pixels, as detailed in Table 1, the trained models were saved into files for subsequent use in predictions. These predictions involved the utilization of separated test images to evaluate and assess the performance of the proposed method.

Tabel 1. Sets of sub-images used in the training of the CNN.

	Class				Total number of sub-images
	Normal	Defect (germinated)			
Germination stages	0h	6h	12h	24h	
No data augmentation	300	300	300	300	1200
With data augmentation	1200	1200	1200	1200	4800

In the experiment, 70% of the images in each set were used for training, 15% for validation, and 15% for testing the CNN.

Data augmentation

To implement data augmentation, two primary image processing operations were applied: rotation and mirroring. The application of this technique substantially increased the number of sub-images available for training, enhancing dataset diversity and significantly improving the

CNN's ability to generalize patterns, ultimately strengthening its capacity to learn from a broader range of examples, as explained in [28, 29]. In our implementation, each original image underwent horizontal and vertical mirroring, along with a fixed-angle rotation of either +90° or –90°, randomly selected. As a result, each original sample produced three distinct augmented variants, leading to a fourfold increase in data volume per category. The amount of augmentation was empirically defined through preliminary experiments, in which we assessed model performance with different augmentation factors. The selected configuration provided a favorable balance between dataset diversity and training stability, effectively enhancing the network's generalization capacity without introducing redundancy or overfitting.

3. RESULTS

The effectiveness of the proposed methodology was evaluated using both LASCA and LASTCA speckle image analysis techniques, followed by CNN-based classification. The results are presented through representative contrast maps, confusion matrices, and quantitative performance metrics. A comprehensive comparison was carried out between the two methods, considering models trained with and without data augmentation.

Figure 6 displays representative LASCA maps in false color for each of the four germination stages analyzed: 0, 6, 12, and 24 hours. These maps illustrate spatial variations in speckle contrast across the surface of the bean samples. Notably, beans at 24 and 12 hours exhibit pronounced changes in spatial contrast patterns, indicative of elevated biological activity related to the germination process. However, the map corresponding to the 0-hour stage shows elevated noise and ambiguous patterns, which may lead to misclassification of non-germinated beans as germinated.

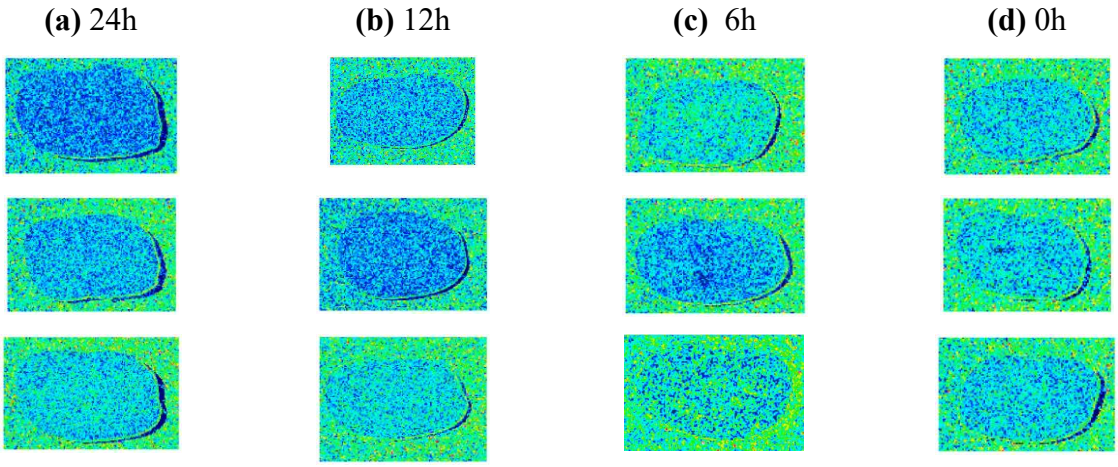

Figure 6. Typical LASCA map of the samples for each germination period.

Figure 7 presents corresponding LASTCA maps, derived from temporal contrast analysis across 120 frames. These maps reveal dynamic variations in speckle intensity over time and offer superior visual discrimination of germination stages. Beans at 24 and 12 hours display regions of high temporal activity, represented by blue and green hues, while the 0-hour sample shows minimal variation, denoted by darker regions. These temporal maps enable more accurate differentiation between germinated and non-germinated grains, particularly at early germination stages.

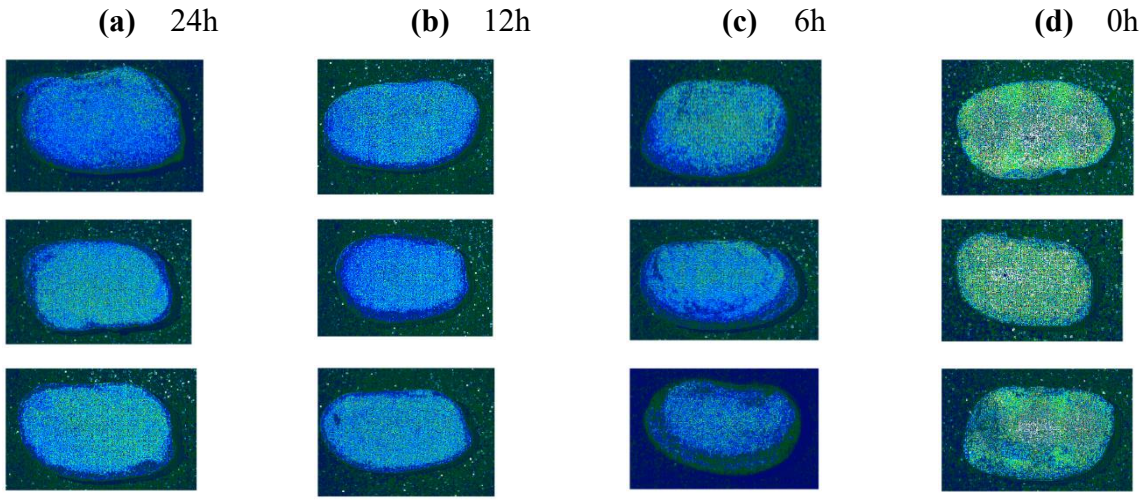

Figure 7. Typical LASTCA map of the samples for each germination period.

Table 2 presents the performance metrics of the CNN classifier trained on LASCA-based speckle images. In this experimental stage, the dataset was segmented by germination intervals to evaluate the classifier's ability to distinguish between non-germinated (0h control group) and germinated beans at each specific stage (6h, 12h, and 24h). Additionally, a final experiment was conducted

using the full set of germination intervals combined (0h, 6h, 12h, and 24h) to assess the model's overall generalization capacity. All tests were carried out under two conditions: with and without the application of data augmentation techniques.

In the absence of data augmentation, the classification accuracy exhibited notable variation depending on the specific germination interval pair analyzed. The most favorable outcome under this condition was observed in the comprehensive experiment encompassing all germination stages, which yielded an overall accuracy of 85.56%, a precision of 82.76%, and a specificity of 96.30%. These results highlight the increased robustness of the CNN model when exposed to a more diverse dataset, even without synthetic data expansion.

When data augmentation was applied—using rotation and mirroring to expand the training dataset—the performance markedly improved. For instance, using only the 0h and 12h samples, the CNN achieved an accuracy of 93.78%, a precision of 96.17%, and a specificity of 96.51%, demonstrating the significant benefit of data augmentation in enhancing model generalization.

Table 2. CNN classifier results obtained by proposed method using LASCA.

	Periods	Precision	Sensitivity	Specificity	Accuracy
Without data augmentation	**0h and 6h**	66.67%	61.54%	66.67%	64.00%
	0h and 12h	51.72%	57.69%	41.67%	50.00%
	0h and 24h	52.38%	42.31%	58.33%	50.00%
	0h, 6h, 12h, and 24h	82.76%	53.33%	96.30%	85.56%
With data augmentation	**0h and 6h**	80.82%	91.24%	79.83%	85.33%
	0h and 12h	96.17%	90.95%	96.51%	93.78%
	0h and 24h	81.28%	83.96%	82.77%	83.33%
	0h, 6h, 12h, and 24h	80.00%	59.65%	94.94%	86.00%

Table 3 presents the classification outcomes using LASTCA-derived maps. Even without data augmentation, the model trained on the complete set of germination periods attained a high accuracy of 91.67%, with a precision of 91.10% and sensitivity of 98.52%. These results underscore the advantage of incorporating temporal information into the contrast analysis, enabling better characterization of dynamic biological activity related to germination.

In scenarios with data augmentation, LASTCA further improved classification performance. The model trained with the full germination set (0h, 6h, 12h, and 24h) achieved the highest overall accuracy of 92.33%, with 98.21% sensitivity, 92.05% precision, and 75.00% specificity. These metrics indicate a strong capacity to correctly identify germinated beans (true positives) while minimizing false negatives.

Table 3. CNN classifier results obtained by proposed method using LASTCA.

	Periods	Precision	Sensitivity	Specificity	Accuracy
Without data augmentation	**0h and 6h**	66,67%	69,57%	70,37%	70,00%
	0h and 12h	62,50%	86,96%	55,56%	70,00%
	0h and 24h	63,33%	76,00%	56,00%	66,00%
	0h, 6h,12h, and 24h	91,10%	98,52%	71,11%	91,67%
With data augmentation	**0h and 6h**	73,36%	88,16%	67,12%	77,78%
	0h and 12h	69,28%	98,15%	59,83%	78,22%
	0h and 24h	58,22%	76,23%	46,26%	61,11%
	0h, 6h,12h, and 24h	92,05%	98,21%	75,00%	92,33%

Figures 8 and 9 provide visual comparisons of CNN classification accuracy across different germination intervals, with and without data augmentation. Figure 8 highlights that LASTCA consistently outperformed LASCA in models trained without data augmentation. Conversely, Figure 9 shows that when data augmentation was applied, LASCA maps approached the accuracy

359 levels of LASTCA, suggesting that sufficient training data can partially compensate for the lack
360 of temporal information.

361 Figure 8 shows the plot of the accuracy of CNN in experiments considering both laser speckle
362 methods, using only the experimental data.

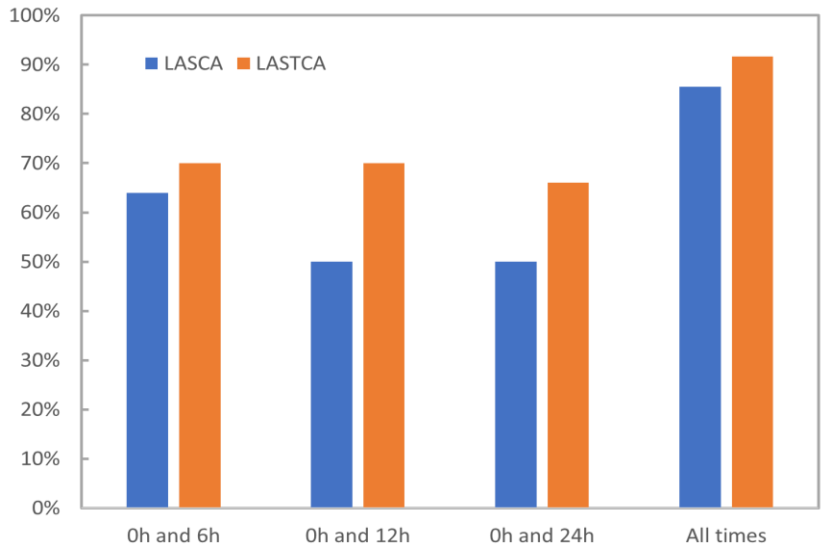

363
364 **Figure 8.** Comparative analysis with the CNN trained without data augmentation.
365
366 Figure 9 shows the plot of the accuracy of CNN in experiments considering both laser speckle
367 methods, using only the augmented data.

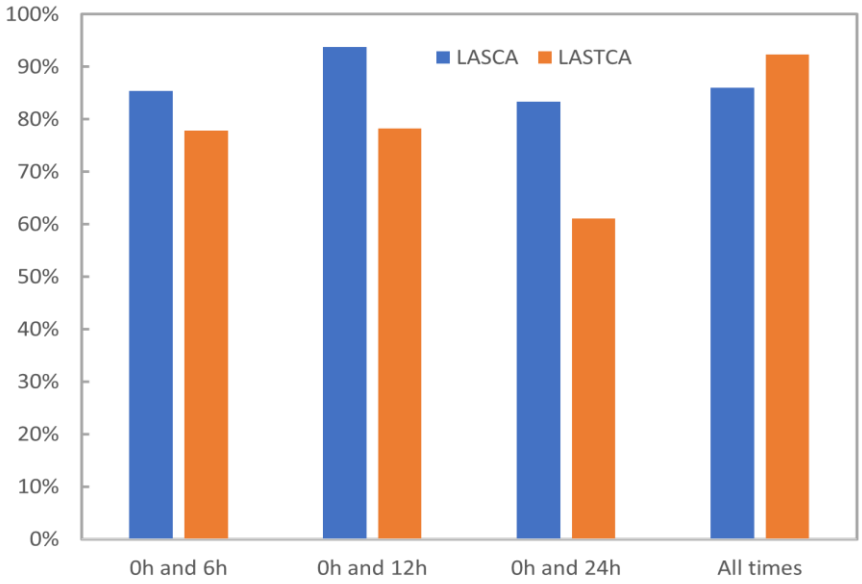

368
369 **Figure 9.** Comparative analysis with the CNN trained with data augmentation.

In addition to the previous experiments, we employed the t-distributed Stochastic Neighbor Embedding (t-SNE) projection method, developed by [30], to visualize the separability of the contrast maps generated by the LASCA and LASTCA approaches. The corresponding visualizations are presented in Figures 10 and 11. For this experiment, the 50×50 pixel sub-images of the training set were vectorized and used as input for t-SNE, which projects the data into a two-dimensional space while preserving the similarity relationships from the original high-dimensional space. The idea is that the feature vectors associated with germination will cluster closely together, thereby enabling a clear visual separation between normal and germinated grain samples.

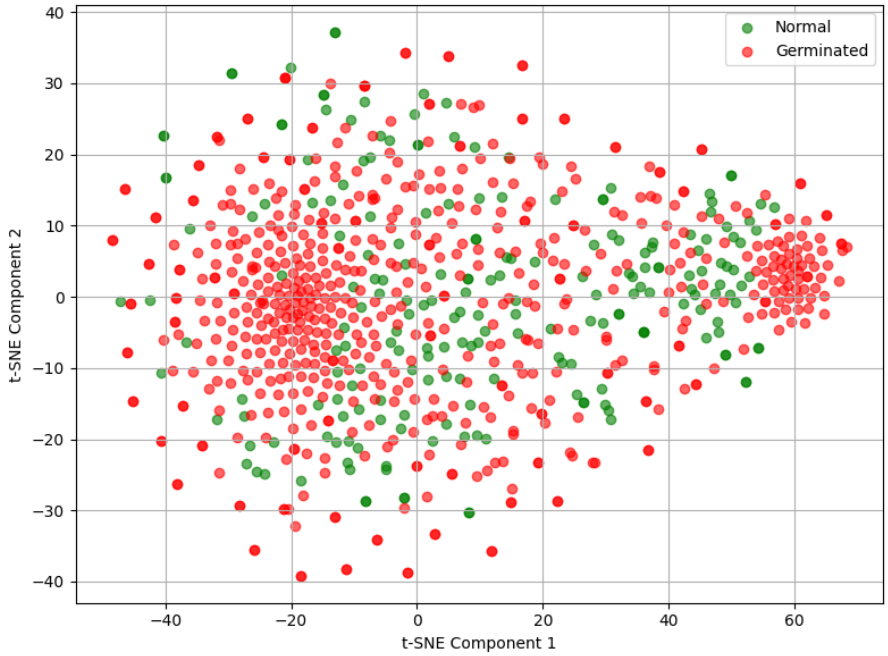

Figure 10. t-SNE clustering of feature vectors extracted from LASCA.

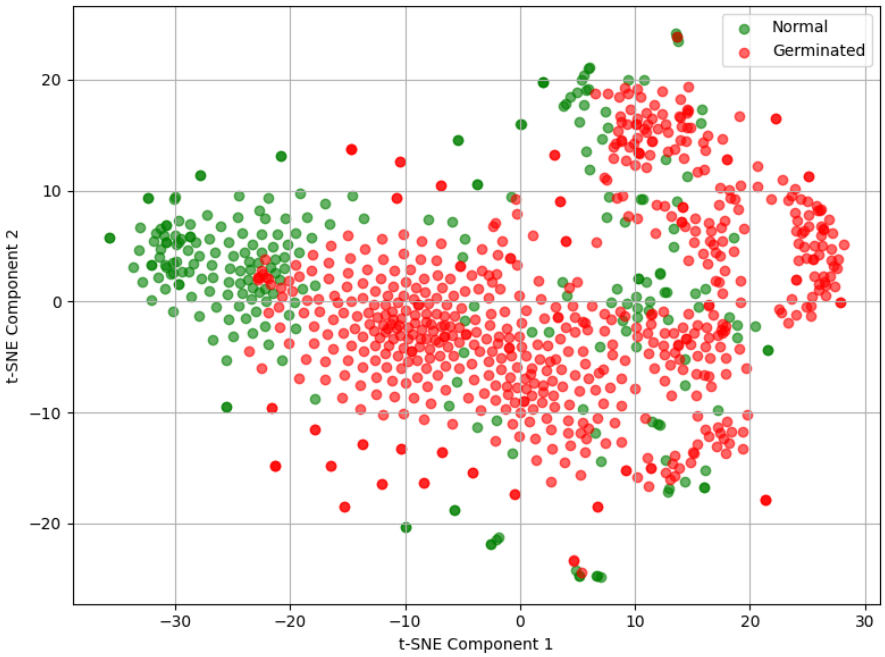

Figure 11. t-SNE clustering of feature vectors extracted from LASTCA.

In Figure 10, it can be observed that the data derived from LASCA do not form well-defined clusters between normal and germinated samples, showing considerable overlap between the two classes in the two-dimensional space. In contrast, Figure 11 reveals a clearer separation between the groups, with dense regions of points corresponding to each class and reduced overlap between normal and germinated data. This result indicates that the use of LASTCA, by incorporating temporal information from speckle activity, provides greater discriminative power in distinguishing patterns associated with germination.

Overall, the results demonstrate that LASTCA provides the most robust and accurate classification of germinated defects. Moreover, the effectiveness of the CNN architecture in processing 50×50 pixel sub-images, and its sensitivity to temporal contrast patterns, reinforces the viability of the proposed approach as a non-invasive, automated tool for quality control in agroindustrial applications.

4. DISCUSSION

In Figure 6, maps representing time intervals of 24, 12, 6, and 0 hours in the developmental stages of beans under laser illumination are displayed, alongside their corresponding false color representations. The false colors aim to enhance visual interpretability and comprehension of

germination dynamics by emphasizing contrast patterns observed in the LASCA (Laser Speckle Contrast Analysis) maps.

It is imperative to underscore the nuanced interpretation divergence between LASCA-derived maps and those generated through the LASTCA (Laser Speckle Temporal Cluster Analysis) method. Within LASCA, the resulting maps signify spatial intensity variations, where decreased activity regions exhibit higher contrast and, consequently, brighter areas. Conversely, regions of heightened activity demonstrate reduced contrast, manifesting as darker zones [23].

The LASTCA-derived maps depicted in Figure 7 delineate temporal intensity fluctuations across 120 frames extracted from an AVI file. These images distinctly showcase areas of differential activity levels—bluish regions denote heightened activity, while the greener areas indicate negligible or dormant activity. LASTCA accentuates areas of increased contrast in more active zones, which consequently portray higher values in the final image.

The comparative analysis between LASCA and LASTCA methods reveals distinct performance in visualizing germination across different time frames. LASCA effectively depicts grain germination in the frames captured at 24, 12, and 6 hours, but encounters challenges in the frames at 0 hours due to noise, causing ambiguity in distinguishing germination from non-germination. Conversely, LASTCA outperforms LASCA, offering clearer, less noisy representations, facilitating visual interpretation, and significantly enhancing the differentiation between germinated and non-germinated grains within the speckle maps derived from 120 frames.

In spatial contrast analysis, the interpretation of maps should consider the signal-to-noise ratio, involving the relative standard deviation of intensities within specific regions. The LASCA maps (Figure 6) exhibit a nuanced challenge: the non-germinated bean area (0h) appears slightly active, potentially leading to misinterpretation and false positives (FP) when analyzing such regions inattentively.

Contrastingly, the LASTCA map (Figure 7) accurately portrays low activity in non-germinated beans, owing to its accumulation of images over time. This temporal aggregation empowers LASTCA to discern and represent actual activity levels more accurately, thus distinguishing germinated from non-germinated regions with higher precision, reducing the occurrence of FP and enhancing the method's reliability in characterizing germination.

The outcomes from the CNN models are delineated through confusion matrices illustrated in Tables 2 and 3, providing insights into the method's accuracy and misclassifications across various

classes. One model was trained without data augmentation, achieving a 91.67% accuracy by correctly predicting 165 out of 180 tests. In contrast, the model trained with data augmentation improved accuracy to 92.33%, with 831 correct predictions out of 900 tests.

The training and validation of models relied on LASTCA-generated maps from 120 frames due to their consistent and higher accuracies observed in experiments, particularly evident when data augmentation was not utilized. Furthermore, the method demonstrated commendable sensitivity, correctly identifying defective grain samples with 98.51% accuracy (133 out of 135) without data augmentation, and 98.21% accuracy (660 out of 672) with data augmentation.

Yet, in experiments employing a set of sub-images of 50×50 pixels derived from LASTCA maps, a noticeable enhancement in the CNN's pattern recognition was observed using the augmented dataset. This discernible improvement is depicted in Table 3, showing improved classification performance. Table 3 further illustrates some classification results with data augmentation, representing normal grains as class 0 and defective (germinated) grains as class 1.

Figures 8 and 9 offer comparative analyses between LASCA and LASTCA methodologies across various germination times. The results highlight the classifier's notably superior performance in identifying grains with shorter germination times, signifying its capability to discern and classify varying germination stages more effectively. This is attributed to the extended germination periods, which result in the prolonged development of the radicle—the part of the bean that centralizes most activity after a specific duration. Consequently, the remainder of the bean becomes less active. The window method utilized in this study might select a region of the bean that is distant from the radicle, potentially causing higher misclassification.

It is crucial to highlight a further increase in accuracy when the LASCA method was combined with data augmentation. This observed enhancement could be attributed to CNN inherently relying on a significant volume of data for robust training. The LASTCA method inherently provides a larger dataset, yet when trained with an identical quantity of data, the network demonstrated superior performance when utilizing the LASCA method. This showcases the heightened contrast achieved by LASCA in characterizing the degree of germination.

An additional advantage of the LASCA method lies in its ability to function with a single image, as opposed to the movie-based requirement of the LASTCA method. In a real production line scenario, this single-image capability could significantly impact the time needed to perform analyses on multiple grains, potentially streamlining the process. Moreover, it's essential to

underscore the method's efficacy in making accurate predictions across different time periods. This robustness indicates that the classifier (CNN) can adeptly manage variations in germination time, establishing itself as a promising tool for identifying germination defects across diverse scenarios.

A computer vision system (CVS) capable of detecting surface-level defects in bean grains, such as fractures, scorched regions, deformation, and mold, was proposed by Belan *et al*. [4], as noted in the introduction of this study. However, that system explicitly excluded the detection of germinated beans, particularly in their early stages. This limitation stems from a fundamental constraint of traditional CVS: it relies solely on visible surface characteristics captured under standard illumination conditions (e.g., RGB imaging). In the early stages of germination, beans typically exhibit no observable external changes—radicle protrusion and structural deformation are not yet apparent. Consequently, visual-based methods cannot access the internal biological activity, such as cellular metabolism or moisture absorption, that precedes external manifestations of germination.

The approach proposed in this study overcomes that deficiency by employing laser speckle imaging (LSI), which is highly sensitive to micro-movements and internal dynamics at the tissue level. Speckle patterns generated under coherent laser illumination contain rich information about subsurface physiological activity, and when analyzed temporally using the LASTCA method, they reveal dynamic fluctuations associated with early germination processes. Unlike CVS, which depends on surface patterns, this technique captures time-resolved biological signals that precede any visible alteration—enabling true non-invasive early detection.

Other studies have applied LSI in agricultural contexts, particularly for viability assessment and fungal contamination monitoring. For example, Singh *et al*. [19] and Thakur et al. [20] used biospeckle activity analysis to evaluate seed vigor and the effects of moisture and temperature on germination in beans and soybeans. Similarly, Rabelo *et al.* [22] demonstrated the use of laser speckle imaging to differentiate bean seeds inoculated with fungi. However, these studies either required manual interpretation of speckle patterns or used classical statistical approaches, lacking automation and robustness for industrial applications. Furthermore, none of them addressed the non-destructive detection of early germinated defects in post-harvest grains, which is critical for consumer-facing quality control.

In contrast, our method introduces several innovations: (1) the use of temporal speckle contrast analysis (LASTCA) to enhance sensitivity to internal activity, (2) the application of convolutional

neural networks (CNNs) for automated classification, and (3) a system architecture that can be scaled for use in industrial grain inspection pipelines. To the best of our knowledge, this is the first study to non-invasively detect early germination defects in beans using deep learning applied to speckle imaging, achieving high accuracy (92.33%) and sensitivity (98.21%) even when no visible signs are present. These contributions represent a significant advancement beyond both traditional CVS and earlier LSI-based research, establishing a new benchmark for intelligent quality control in the agroindustry.

Limitations of the study

Despite the promising results obtained in this study, some limitations related to method validation must be acknowledged. The experiments were conducted under controlled laboratory conditions using a fixed-wavelength laser (633 nm), and the influence of variations in ambient lighting, bean varieties, and environmental humidity was not extensively explored. However, it is important to highlight that laser speckle imaging (LSI) is inherently a coherent and active optical technique, meaning that the speckle pattern depends solely on the properties of the laser source and the sample, rather than on ambient lighting. In fact, laser light is much brighter than ambient light which contributes negligibly to the back-scattered light captured by the camera. The speckle contrast—both spatial (LASCA) and temporal (LASTCA)—is dictated by the microstructural dynamics and scattering properties of the sample, which are modulated by biological activity rather than environmental illumination. This makes LSI particularly robust and reproducible, even under moderately varying acquisition environments, provided that laser alignment and imaging geometry are maintained.

Regarding the generalization to different bean varieties and growth environments, it is indeed true that optical scattering properties may vary between cultivars due to differences in seed coat thickness, pigmentation, or hydration response. Nonetheless, the biological mechanisms underlying germination—including water absorption, metabolic activation, and intracellular motion—are physiologically conserved across legume species. Although the timing of the germination process varies across different species or even withing different types of beans, these processes generate dynamic fluctuations in refractive index and intracellular movement, which manifest as measurable speckle activity regardless of variety. Prior studies in biospeckle imaging

of maize, soybean, and bean seeds (e.g., Singh *et al.* [19]; Silva *et al.* [13]) have confirmed the universality of this principle.

Future works

Further validation using multi-varietal datasets, as well as acquisition under field-like conditions, is a logical next step to confirm the CNN model's transferability. Future studies should aim to assess intra- and inter-species generalization, test the system's tolerance to changes in humidity and temperature, and evaluate the stability of contrast metrics in semi-industrial environments. However, it is worth emphasizing that the core optical signal—the speckle fluctuation caused by biological activity—is fundamentally robust, and the integration with deep learning allows for adaptive pattern recognition that is, by design, capable of learning variation across samples. Therefore, while further validation is necessary for large-scale deployment, the current findings provide a strong foundation and demonstrate the feasibility, sensitivity, and industrial potential of the method.

5. CONCLUSIONS

The integration of speckle image analysis with CNNs led to the development of a cost-effective and computationally efficient approach to identify early stages of germinated defects in bean grains. Throughout the conducted experiments, with and without data augmentation, the method achieved high accuracy rates (91.67% and 92.33%) and sensitivity (98.51% and 98.21%) in identifying the inspected defects. This suggests the method's potential for enhancing the quality control process of beans, providing an alternative to traditional, more expensive automatic inspection equipment. However, it's essential to note that to enhance feasibility and scalability, the method relies on compact hardware comprising a laser, camera, and processor—a potential inspiration for future research endeavors in engineering and computing domains. Finally, by promoting improvements in the agricultural grain quality inspection process, the proposed method contributes to global efforts to achieve the United Nations Sustainable Development Goals (SDGs), in particular SDGs 2 (Zero Hunger), 9 (Industry, Innovation and Infrastructure) 12 (Sustainable Consumption and Production).

DATA AND CODE AVAILABILITY STATEMENTS

The dataset used in this study is publicly available at the following GitHub repository: https://github.com/eliveigajr/Speckle-Images. This repository contains speckle sub-images with dimensions of 50×50 pixels extracted from contrast maps generated by LASCA and LASTCA techniques, as described in Section 2.1. The Python code developed in this study can be provided upon reasonable request.

ACKNOWLEDGMENTS

The authors would like to thank the Conselho Nacional de Desenvolvimento Científico e Tecnológico (CNPq) for awarding research scholarships to A.M.D. and S.A.A. (Processes 304853/2024-0 and 313484/2025-2), FAPESP grant 15/25180-7 as well as the Universidade Nove de Julho (UNINOVE) for their continued institutional support.

REFERENCES

[1] Vargas-Canales, J. M., Brambila-Paz, J. D. J., Pérez-Cerecedo, V., Rojas-Rojas, M. M., López-Reyna, M. D. C., & Omaña-Silvestre, J. M. (2022). Trends in science, technology, and innovation in the agri-food sector. Tapuya: Latin American Science, Technology and Society, 5(1), 2115829.

[2] EMBRAPA – Manual de Classificação do Feijão Instrução Normativa n° 12, de 28 de março de 2008. [s.l.: s.n.], 2012. Disponível em: <www.cnpaf.embrapa.br>.

[3] MAPA – Ministério da Agricultura Pecuária e Abastecimento. disponível em: <http://www.agricultura.gov.br/>, Acesso em: 04 maio 2018.

[4] Belan, P. A., de Macedo, R. A. G., Alves, W. A. L., Santana, J. C. C., & Araujo, S. A. (2020). Machine vision system for quality inspection of beans. The International Journal of Advanced Manufacturing Technology, 111, 3421-3435.

[5] Deana, A. M., Jesus, S. H. C., Koshoji, N. H., Bussadori, S. K., & Oliveira, M. T. (2013). Detection of early carious lesions using contrast enhancement with coherent light scattering (speckle imaging). Laser Physics, 23(7), 075607.

[6] Koshoji, N. H., Bussadori, S. K., Bortoletto, C. C., Prates, R. A., Oliveira, M. T., & Deana, A. M. (2015). Laser speckle imaging: a novel method for detecting dental erosion. PloS one, 10(2), e0118429.

[7] Olivan, S. R. G., Sfalcin, R. A., Fernandes, K. P. S., Ferrari, R. A. M., Horliana, A. C. R. T., Motta, L. J., ... & Bussadori, S. K. (2020). Preventive effect of remineralizing materials on dental

586 erosion lesions by speckle technique: an in vitro analysis. Photodiagnosis and photodynamic
587 therapy, 29, 101655.
588 [8] Ansari, M. Z., Da Silva, L. C., Da Silva, J. V. P., & Deana, A. M. (2016). Modelling laser
589 speckle photographs of decayed teeth by applying a digital image information technique. Laser
590 Physics, 26(9), 095602.
591 [9] Gavinho, L. G., Araujo, S. A., Bussadori, S. K., Silva, J. V., & Deana, A. M. (2018). Detection
592 of white spot lesions by segmenting laser speckle images using computer vision methods. Lasers
593 in Medical Science, 33, 1565-1571.
594 [10] Olivan, S. R. G., Deana, A. M., Pinto, M. M., Sfalcin, R. A., Fernandes, K. P. S., Mesquita-
595 Ferrari, R. A., ... & Bussadori, S. K. (2017). Diagnosis of occlusal caries lesions in deciduous
596 molars by coherent light scattering pattern speckle. Photodiagnosis and Photodynamic Therapy,
597 18, 221-225.
598 [11] Koshoji, N. H., Prates, R. A., Bussadori, S. K., Bortoletto, C. C., de Miranda Junior, W. G.,
599 Librantz, A. F., ... & Deana, A. M. (2016). Relationship between analysis of laser speckle image
600 and Knoop hardness on softening enamel. Photodiagnosis and Photodynamic Therapy, 15, 139-
601 142.
602 [12] Silva, J. V. P. D., Sfalcin, R. A., Andrianarijaona, V. M., Gavinho, L. G., Salviatto, L. T. C.,
603 Bussadori, S. K., & Deana, A. M. (2020). Detection of carious lesion by laser speckle analysis
604 using the first order moment.
605 [13] Silva, G. M., Peixoto, L. S., Fujii, A. K., Parisi, J. J. D., Aguiar, R. H., & Fracarolli, J. A.
606 (2018). Evaluation of maize seeds treated with Trichodermil® through biospeckle. Journal of
607 Agricultural Science and Technology, 8, 175-187..
608 [14] Peixoto, L. S., Silva, G. M., Fujii, A. K., Parisi, J. J. D., Aguiar, R. H., & Fracarolli, J. A.
609 (2018). Maize Seeds Submitted to Thermotherapy and Analyzed by Dynamic Speckle. Journal of
610 Agricultural Science and Technology B, 8(2), 115-121.
611 [15] Xia, Y., Xu, Y., Li, J., Zhang, C., & Fan, S. (2019). Recent advances in emerging techniques
612 for non-destructive detection of seed viability: A review. Artificial Intelligence in Agriculture, 1,
613 35-47.
614 [16] Singh, P., Chatterjee, A., Bhatia, V., & Prakash, S. (2020). Application of laser biospeckle
615 analysis for assessment of seed priming treatments. Computers and electronics in agriculture, 169,
616 105212.

[17] Kurokawa e Silva, G., Aguiar, R. H., Oliveira, R. A. D., & Fabbro, I. M. D. (2020). Indirect determination of moisture using biospeckle technique. Revista Ciência Agronômica, 51.

[18] Contado, J. L., de Faria Silva, C., & Júnior, R. A. B. (2020). BIOSPECKLE LASER TO MONITOR THE GERMINATION OF ANGICO-VERMELHO SEEDS. Theoretical and Applied Engineering, 4(4), 1-9.

[19] Singh, P., Chatterjee, A., Bhatia, V., & Prakash, S. (2018, November). Viability Assessment of Kidney Bean Seed (Phaseolus Vulgaris sp.) Using Robust Biospeckle Indexing Technique. In Workshop on Computational Models of Natural Argument (pp. 189-195). Singapore: Springer Singapore.

[20] Thakur, P. S., Chatterjee, A., Rajput, L. S., Rana, S., Bhatia, V., & Prakash, S. (2022). Laser biospeckle technique for characterizing the impact of temperature and initial moisture content on seed germination. Optics and Lasers in Engineering, 153, 106999.

[21] Braga Jr, R. A., Rabelo, G. F., Granato, L. R., Santos, E. F., Machado, J. C., Arizaga, R. & Trivi, M. (2005). Detection of fungi in beans by the laser biospeckle technique. Biosystems engineering, 91(4), 465-469.

[22] Rabelo, G. F., Enes, A. M., Junior, R. A. B., & Dal Fabbro, I. M. (2011). Frequency response of biospeckle laser images of bean seeds contaminated by fungi. Biosystems engineering, 110(3), 297-301.

[23] Goodman, J. W. (1975). Statistical properties of laser speckle patterns. In Laser speckle and related phenomena (pp. 9-75). Berlin, Heidelberg: Springer Berlin Heidelberg.

[24] Gavinho, L. G., Araujo, S. A., Bussadori, S. K., Silva, J. V., & Deana, A. M. (2018). Detection of white spot lesions by segmenting laser speckle images using computer vision methods. Lasers in Medical Science, 33(7), 1565-1571.

[25] Deana, A. M., Jesus, S. H. C., Koshoji, N. H., Bussadori, S. K., & Oliveira, M. T. (2013). Detection of early carious lesions using contrast enhancement with coherent light scattering (speckle imaging). Laser Physics, 23(7), 075607.

[26] Koshoji, N. H., Bussadori, S. K., Bortoletto, C. C., Prates, R. A., Oliveira, M. T., & Deana, A. M. (2015). Laser speckle imaging: a novel method for detecting dental erosion. PloS one, 10(2), e0118429.

[27] Briers, J. D., & Webster, S. (1996). Laser speckle contrast analysis (LASCA): a nonscanning, full-field technique for monitoring capillary blood flow. Journal of biomedical optics, 1(2), 174-179.

[28] Bravo, D. T., Lima, G. A., Alves, W. A. L., Colombo, V. P., Djogbenou, L., Pamboukian, S. V. D., & de Araujo, S. A. (2021). Automatic detection of potential mosquito breeding sites from aerial images acquired by unmanned aerial vehicles. Computers, Environment and Urban Systems, 90, 101692.

[29] Shorten, C., & Khoshgoftaar, T. M. (2019). A survey on image data augmentation for deep learning. Journal of big data, 6(1), 1-48.

[30] Maaten, L. V. D., & Hinton, G. (2008). Visualizing data using t-SNE. *Journal of machine learning research*, *9*(Nov), 2579-2605.